Inorg. Chem. **2008**, *47*, 2338−2346

Homoleptic, Four-Coordinate Azadipyrromethene Complexes of d^{10} Zinc and Mercury

Thomas S. Teets, David V. Partyka, James B. Updegraff III, and Thomas G. Gray*

Department of Chemistry, Case Western Reserve University, Cleveland, Ohio 44106

Received June 18, 2007

Tetraarylazadipyrromethenes, and especially their boron chelates, are a growing class of chromophores that are photoactive toward red light. The coordination chemistry of these ligands remains to be explored. Reported here are four-coordinate zinc(II) and mercury(II) complexes of tetraarylazadipyrromethene ligands. The new complexes contain two azadipyrromethenes bound per d^{10} metal center and are characterized by ^{1}H NMR, optical absorption spectroscopy, X-ray diffraction crystallography, and elemental analysis. Solid-state structures show that these bis-chelate complexes distort significantly from idealized D_{2d} symmetry. AM1 geometry optimizations indicate relaxation energies in the range of 6.8–15.2 kcal mol^{-1}; interligand π-stacking provides an added energetic impetus for distortion. The absorption spectra show a marked increase in the absorption intensity in the red region and, in the case of the zinc(II) complexes, the development of a second distinct absorption band in this region, which is red-shifted by ca. 40–50 nm relative to the free ligand. Semiempirical INDO/S computations indicate that these low-energy optical absorptions derive from allowed excitations among ligand-based orbitals that derive from the highest occupied molecular orbital and lowest unoccupied molecular orbital of the free azadipyrromethene.

Introduction

Azadipyrromethenes are an emerging class of bidentate organic ligands that have occasioned scrutiny because of their absorption of red and near-infrared light. In particular, BF_2^+ chelates of aryl-substituted azadipyrromethenes possess favorable properties for a variety of bio-optical applications.[1–6] Figure 1a depicts the general structure of symmetrical BF_2−azadipyrromethenes.

Boron azadipyrromethenes generally show intense absorption in the red region of the spectrum ($\lambda_{max} > 650$ nm), with $\epsilon \sim 75\,000-85\,000$ M^{-1} cm^{-1}. Several have also been shown to be luminescent at room temperature; the tetraphenyl compound ($Ar_1 = Ar_2 = Ph$) emits at 672 nm with a fluorescence quantum yield $\Phi_F = 0.34$.[1] The absorption and emission profiles of these chromophores are readily tuned by altering the substitution of the aryl groups; electron-donating groups[2,3] such as −OMe and $-NR_2$ as well as conformationally restricted substituents[4] red-shift both the absorption and emission profiles. BF_2^+ chelates of dimethylamino-substituted tetraarylazadipyrromethenes,[3] where Ar_1 = *p*-*N*,*N*-dimethylaniline in Figure 1a, have been shown to be efficient pH sensors. Terminal substitution with diethylamine or morpholine functionalities produces photoinduced electron-transfer-modulated sensors that respond to changes in pH and microenvironmental polarity.[1] Efficient mercury(II) sensing was achieved through incorporation of *o*-pyridyl donors onto the ligand scaffold,[5] at the "Ar_1" position of Figure 1a. In addition, boron azadipyrromethenes,

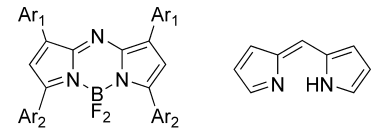

Figure 1. Structures of (a) the BF_2^+ chelate of a tetraarylazadipyrromethene and (b) unsubstituted dipyrrin.

* To whom correspondence should be addressed. E-mail: tgray@case.edu.

(1) Hall, M. J.; Allen, L. T.; O'Shea, D. F. *Org. Biomol. Chem.* **2006**, *4*, 776–780.
(2) Gorman, A.; Killoran, J.; O'Shea, C.; Kenna, T.; Gallagher, W. M.; O'Shea, D. F. *J. Am. Chem. Soc.* **2004**, *126*, 10619–10631.
(3) McDonnell, S. O.; O'Shea, D. F. *Org. Lett.* **2006**, *8*, 3493–3496.
(4) Zhao, W.; Carreira, E. M. *Angew. Chem., Int. Ed.* **2005**, *44*, 1677–1679*Chem.*−*Eur. J.* **2006**, *12*, 7254–7263.
(5) Coskun, A.; Yilmaz, M. D.; Akkaya, E. U. *Org. Lett.* **2007**, *9*, 607–609.
(6) (a) Gallagher, W. M.; Allen, L. T.; O'Shea, C.; Kenna, T.; Hall, M.; Gorman, A.; Killoran, J.; O'Shea, D. F. *Br. J. Cancer* **2005**, *92*, 1702–1710. (b) McDonnell, S. O.; Hall, M. J.; Allen, L. T.; Byrne, A.; Gallagher, W. M.; O'Shea, D. F. *J. Am. Chem. Soc.* **2005**, *127*, 16360–16361. (c) Killoran, J.; Allen, L.; Gallagher, J. F.; Gallagher, W. M.; O'Shea, D. F. *Chem. Commun.* **2002**, 1862–1863.

10.1021/ic701190g CCC: $40.75
Published on Web 02/27/2008

Scheme 1. Syntheses of **2a**−**c** and **3**

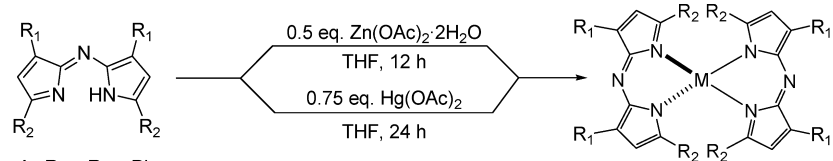

1a $R_1 = R_2 =$ Ph
1b R_1 = Ph, $R_2 = p$-C_6H_4OMe
1c $R_1 = p$-C_6H_4OMe, R_2 = Ph

2a M = Zn; $R_1 = R_2$ = Ph: 84%
2b M = Zn; R_1 = Ph, $R_2 = p$-C_6H_4OMe: 90%
2c M = Zn; R_1 p-C_6H_4OMe, R_2 = Ph: 54%
3 M = Hg; $R_1 = R_2$ = Ph: 61%

where pyrrolic protons are substituted with bromine, are efficient sensitizers of oxygen,[2,6] making them a target of interest for a new class of nonporphyrin photodynamic therapy mediators.

Four-coordinate bis-chelates of the related dipyrromethene ligand, containing a variety of 2+ metal ions, are abundant.[7] The structure of the dipyrromethene ligand, often referred to as "dipyrrin", is shown in Figure 1b. The pyrrolic carbons and the bridging meso carbon can be functionalized with a variety of substituents, leading to numerous possible architectures.

Dipyrrinato bis-chelates of zinc(II) have been obtained as side products during templated syntheses of zinc(II) porphyrins.[8] In recent years, numerous homoleptic bis(dipyrrinato) complexes have been prepared and studied, employing a variety of metal ions and encompassing several geometries. Recent efforts have produced homoleptic bis-chelate complexes of zinc(II)[9] and nickel(II)[10] and also tris-chelates of group 13 metals,[11] iron(III) and cobalt(III).[12] Dipyrromethene complexes of zinc(II),[13] copper(II)[14] and cobalt(II)[15] have been examined in the context of supramolecular chemistry, as synthons for coordination polymers having significant electronic, optical, and magnetic properties. Another recent trend is the development of porphyrin−dipyrromethene oligomers,[16] which are targeted for use in efficient light-harvesting arrays. The coordination chemistry of dipyrromethenes, which are structurally similar to azadipyrromethenes, has been pursued extensively.

The metallocomplex chemistry of azadipyrromethenes has been slower to develop. Free azadipyrromethenes are isolated before boronation, so the opportunity to incorporate metals into the ligand framework is readily apparent. Heavy-atom binding to the azadipyrromethene core is one means of attuning the ligand photophysics and of accessing photoreactivity from its triplet excited states.

Reported here is a series of four-coordinate zinc(II) and mercury(II) bis-chelate complexes of tetraarylazadipyrromethenes. The new compounds were characterized by ^{1}H NMR, optical absorption spectroscopy, and elemental analysis; all but one were structurally characterized by single-crystal X-ray diffraction. Absorption in the red region greatly intensifies in the complexes relative to the free azadipyrromethene, with a second distinct absorption transition evident in this region for the zinc(II) compounds. The complexes also demonstrate intramolecular π-stacking interactions both in the solid state and in solution. We believe these interactions stabilize the observed structures, which are significantly distorted from D_{2d} symmetry.

Results and Discussion

Synthesis. To prepare the zinc(II) complexes **2a**−**c**, zinc(II) acetate dihydrate was reacted with 2 equiv of tetraarylazadipyrromethenes **1a**−**c** in tetrahydrofuran (THF) to yield the appropriate homoleptic complexes as crystalline solids in good to excellent isolated yields, ranging from 54% to 90% (Scheme 1).

Upon mixing, an instantaneous color change occurs to a brighter, more greenish-blue tint relative to the free ligand. Quantitative conversion was observed with 12 h reaction times. In the case of **2c**, heating at 40 °C was required to ensure complete reaction; at room temperature, a small amount of free ligand was observed in the ^{1}H NMR spectra of the product. The products were recrystallized by vapor diffusion of pentane into THF solutions, which afforded the complexes in good purity as judged by ^{1}H NMR and elemental analysis. The mercury(II) complex **3** was prepared in an analogous manner by direct reaction of **1a** and mercury(II) acetate in THF. However, a slight excess of the mercury salt, 0.75 equiv rather than the stoichiometric 0.5 equiv, and longer reaction time, 24 h rather than 12 h, were required for the reaction to reach completion. Product **3** was

(7) Wood, T. E.; Thompson, A. *Chem. Rev.* **2007**, *107*, 1831–1861.
(8) Marchon, J. C.; Ramasseul, R.; Ulrich, J. *J. Heterocycl. Chem.* **1987**, *24*, 1037–1039.
(9) (a) Sazanovich, I. V.; Kirmaier, C.; Hindin, E.; Yu, L.; Bocian, D. F.; Lindsey, J. S.; Holten, D. *J. Am. Chem. Soc.* **2004**, *126*, 2664–2665. (b) Brückner, C.; Karunaratne, V.; Rettig, S. J.; Dolphin, D. *Can. J. Chem.* **1996**, *74*, 2182–2193. (c) Halper, S. R.; Stork, J. R.; Cohen, S. M. *Dalton Trans.* **2007**, 1067–1074.
(10) Clarke, E. T.; Squattrito, P. J.; Rudolf, P. R.; Motekaitis, R. J.; Martell, A. E.; Clearfield, A. *Inorg. Chim. Acta* **1989**, *166*, 221–231.
(11) Thoi, V. S.; Stork, J. R.; Magde, D.; Cohen, S. M. *Inorg. Chem.* **2006**, *45*, 10688–10697.
(12) Halper, S. R.; Cohen, S. M. *Inorg. Chem.* **2005**, *44*, 486–488.
(13) (a) Maeda, H.; Hasegawa, M.; Hashimoto, T.; Kakimoto, T.; Nishio, S.; Nakanishi, T. *J. Am. Chem. Soc.* **2006**, *128*, 10024–10025. (b) Wood, T. E.; Ross, A. C.; Dalgleish, N. D.; Power, E. D.; Thompson, A.; Chen, X.; Okamoto, Y. *J. Org. Chem.* **2005**, *70*, 9967–9974. (c) Thompson, A.; Dolphin, D. *J. Org. Chem.* **2000**, *65*, 7870–7877.
(14) (a) Do, L.; Halper, S. R.; Cohen, S. M. *Chem. Commun.* **2004**, *23*, 2662–2663. (b) Halper, S. R.; Cohen, S. M. *Angew. Chem., Int. Ed.* **2004**, *43*, 2385–2388. (c) Heinze, K.; Reinhart, A. *Inorg. Chem.* **2006**, *45*, 2695–2703.
(15) Zhang, Y.; Thompson, A.; Rettig, S. J.; Dolphin, D. *J. Am. Chem. Soc.* **1998**, *120*, 13537–13538.
(16) (a) D'Souza, F.; Smith, P. M.; Zandler, M. E.; McCarty, A. L.; Itou, M.; Araki, Y.; Ito, O. *J. Am. Chem. Soc.* **2004**, *126*, 7898–7907. (b) Yu, L.; Muthukumaran, K.; Sazanovich, I. V.; Kirmaier, C.; Hindin, E.; Diers, J. R.; Boyle, P. D.; Bocian, D. F.; Holten, D.; Lindsey, J. S. *Inorg. Chem.* **2003**, *42*, 6629–6647.

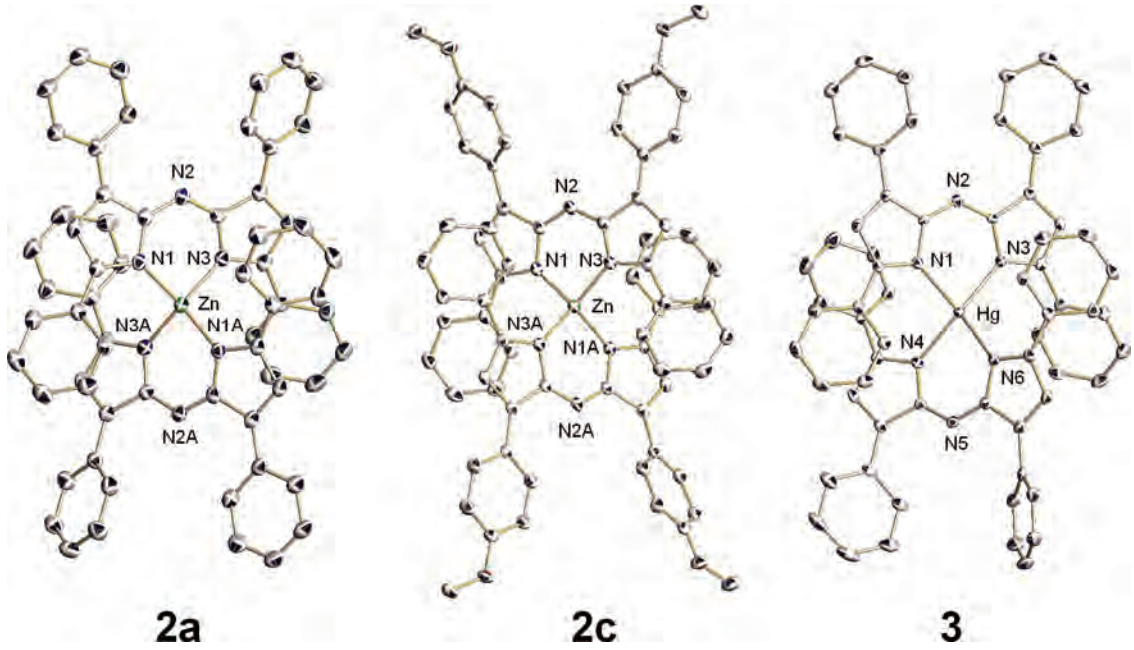

Figure 2. Crystal structures of **2a**, **2c**, and **3** with partial labeling schemes and 50% probability ellipsoids. Hydrogen atoms are omitted for clarity, and carbon atoms are not labeled. Data were collected at 100 ± 2 K.

isolated in 61% yield. Attempts at the synthesis of cadmium analogues of **2** and **3** produced intractable mixtures of the free ligand and complex.

^{1}H NMR readily establishes the formation of bis(azadipyrromethene) complexes. When measured in $CDCl_3$, the singlet associated with the pyrrolic protons shifts upfield by 0.4–0.5 ppm in the zinc(II) complexes relative to the free ligand. One of the aromatic doublets associated with the proximal azadipyrromethene phenyl rings (i.e., the phenyl substituents deriving from acetophenone)[2] exhibits an upfield shift of the same magnitude in the complexes. Furthermore, in **2b**, the methoxy singlet shifts upfield by 0.55 ppm. The remaining ligand peaks are generally unresponsive to complex formation, shifting by <0.1 ppm upon the formation of zinc(II) complexes. The ^{1}H NMR spectrum of **3** is very similar to that of **2a**, but the upfield shift of the pyrrolic proton resonance is smaller, only shifting ~0.2 ppm in **3** relative to **1a**.

Crystal Structures. Irregular, block-shaped crystals of **2a**, **2c**, and **3** were grown from concentrated THF solutions by vapor diffusion of pentane at room temperature; attempts to grow X-ray-quality crystals of **2b** resulted in fibrous needles that were too thin to mount on a goniometer. Figure 2 depicts crystal structures of **2a**, **2c**, and **3**. Table 1 collects crystallographic data.

Compound **2a** crystallized in the orthorhombic space group *Fdd*2; **2c** crystallized in the monoclinic space group *C*2/*c*, and **3** crystallized in the orthorhombic space group $P2_12_12_1$. Molecules of **2a** and **2c** reside on crystallographically imposed C_2 axes such that the asymmetric unit consists of the zinc atom and one azadipyrromethene ligand. Table 2 summarizes relevant interatomic distances and angles for **2a**, **2c**, and **3**.

The Zn−N bond lengths, which range between 1.984(2) and 1.9905(13) Å, are unremarkable and, in general, similar to those found in structurally characterized zinc(II) dipyrrin complexes.[9c,16b] The ligand bite angles, defined as ∠N−M−N, are 94.56(8)° for **2a** and 96.44(13)° for **2c**; again these values are comparable to those for zinc dipyrrin complexes. The bite angles in **3** are smaller at 87.11(7)° and 86.51(7)°. This decrease in the bite angle within increasing radius of the metal atom mirrors the trend observed for previously reported coinage metal complexes of azadipyrromethenes.[17] Backbone $C-N_{meso}-C$ bond angles, where N_{meso} is the bridging nitrogen atom not involved in metal ligation, are larger than those reported for two BF_2−azadipyrromethenes.[2,6c] With the smaller boron atoms in the ligand pocket, the $C-N_{meso}-C$ bond angles are 119.7(3)° and 119.5(3)°, while in the metal(II) bis-chelates reported here, the angle has widened to 126.3(2)° for **2a**, 127.93(14)° for **2c**, and 128.5(2)° and 129.5(3)° for **3**. These larger angles indicate sufficient flexibility in the ligand backbone to allow distortion from ideal sp^2 hybridization at nitrogen upon metal-ion binding. As with the other structural parameters, these angles in **2a** and **2c** are comparable to analogous $C-C_{meso}-C$ angles in zinc dipyrrinato complexes. The most notable structural difference in **3** compared to **2a** and **2c** is an asymmetry in Hg−N bond lengths for each chelated azadipyrromethene; the two lengths are nearly equal in the zinc(II) complexes; see Table 1. The two six-membered chelate rings in **3** each consist of one long Hg−N bond and one short Hg−N bond, which differ by more than 0.2 Å. This asymmetry likely reflects a mismatch between the size of the mercury(II) cation and the ligand cavity.

The coordination geometries of **2a**, **2c**, and **3** distort significantly from D_{2d} symmetry, as indicated by the angle between best-fit planes of the two six-membered chelate rings. This angle is 63.50° in **2a**, 68.67° in **2c**, and 67.91°

(17) Teets, T. S.; Partyka, D. V.; Esswein, A. J.; Updegraff, J. B.; Zeller, M.; Hunder, A. D.; Gray, T. G. *Inorg. Chem.* **2007**, *46*, 6218–6220.

Table 1. Crystallographic Data for **2a**, **2c**, and **3**

	2a	**2c**	**3**
formula	$C_{64}H_{44}N_6Zn$	$C_{68}H_{52}N_6O_4Zn$	$C_{68}H_{52}HgN_6O$
fw	962.42	1082.53	1169.79
cryst syst	orthorhombic	monoclinic	orthorhombic
space group	*Fdd*2	*C*2/*c*	$P2_12_12_1$
a, Å	19.8576(11)	21.149(6)	12.2174(9)
b, Å	44.419(2)	10.888(3)	15.6645(12)
c, Å	10.8128(5)	22.737(5)	27.527(2)
α, deg			
β, deg		94.700(5)	
γ, deg			
cell volume, Å^3	9537.6(8)	5218(2)	5268.2(7)
Z	8	4	4
D_{calcd}, Mg, m^3	1.340	1.378	1.475
T, K	100 ± 2	100 ± 2	100 ± 2
μ, mm^{-1}	0.565	0.531	2.974
F(000)	4000	2256	2360
cryst size, mm	0.41 × 0.29 × 0.16	0.28 × 0.16 × 0.14	0.42 × 0.39 × 0.22
$\theta_{min}-\theta_{max}$, deg	1.83−27.34	1.80−27.50	1.82−27.50
no. of reflns collected	58 263	29 971	60 315
no. of indep reflns	5402	5987	12057
no. of refined param	321	359	685
GOF[a] on F^2	0.971	1.040	1.000
final *R* indices[b] [$I > 2\sigma(I)$]			
R1	0.0388	0.0339	0.0187
wR2	0.1065	0.0800	0.0420
R indices (all data)			
R1	0.0498	0.0443	0.0225
wR2	0.1192	0.0854	0.0430

[a] GOF = $[\sum w(F_o^2 - F_c^2)^2/(n-p)]^{1/2}$; n = number of reflections, p = number of parameters refined. [b] R1 = $\sum(||F_o| - |F_c||)/\sum|F_o|$; wR2 = $[\sum w(F_o^2 - F_c^2)^2/\sum wF_o^4]^{1/2}$.

Table 2. Selected Interatomic Distances (Å) and Angles (deg) for **2a**, **2c**, and **3**

	2a	**2c**	**3**
M−N1	1.984(2)	1.9882(14)	2.3642(19)
M−N3	1.987(2)	1.9905(13)	2.0971(17)
M−N4	N/A	N/A	2.1086(18)
M−N6	N/A	N/A	2.3297(18)
N−M−N (bite angle)	94.56(8)	96.44(5)	87.11(7), 86.51(7)
C−N_{meso}−C	126.3(2)	127.93(14)	129.5(3), 128.5(2)
Θ[a]	63.50	68.67	67.91

[a] Dihedral angle between six-membered chelate rings.

in **3**, leading to a distorted tetrahedral arrangement of donor nitrogen atoms at the metal center. The structures of **2a** and **2c** approximate D_2 symmetry. Figure 3a shows a "top" view of the structure of **2a**, looking down the $N_{meso}-Zn-N_{meso}$ axis, clearly showing the deviation from D_{2d} symmetry in the complex. The planes shown in Figure 3a represent best-fit planes of the two chelate rings.

We propose that intramolecular π-stacking is an essential contributor to the crystallographically observed geometry. In the solid state, the pyrrole ring of one of the azadipyrromethenes aligns parallel to and within π-stacking distance of a proximal phenyl ring on the opposite azadipyrromethene ligand. In **2a**, a minimum distance of 3.629 Å is observed between the centroids of adjacent rings; in **3**, an even shorter contact of 3.602 Å is observed, while in **2c**, the smallest such distance is 3.942 Å, which indicates more limited interaction, if any. Figure 3b shows another view of **2a**, where the stacking interaction is apparent.

NMR spectra of the complexes indicate that π-stacking interactions persist in solution. As previously mentioned, the ^{1}H NMR resonances of the pyrrolic protons and the proximal phenyl rings (i.e., the phenyl substituents deriving from

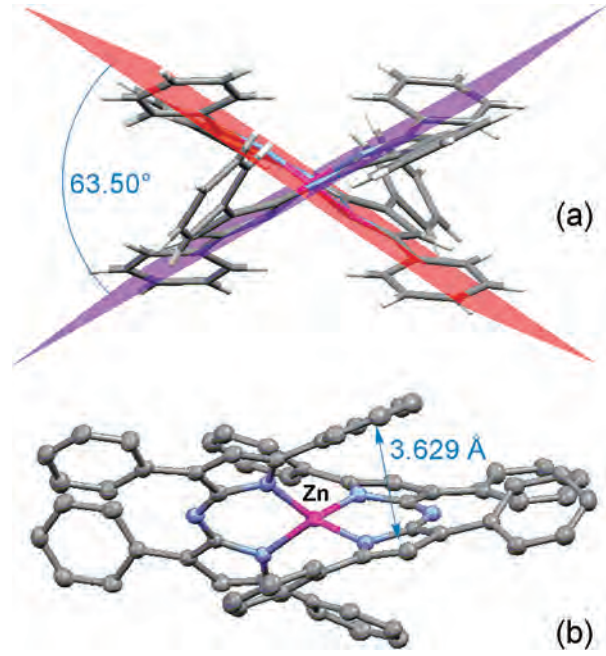

Figure 3. (a) Crystal structure of **2a** illustrating the dihedral angle between best-fit planes of the two six-membered chelate rings. (b) View of the crystal structure of **2a** showing π-stacking between the proximal phenyl group of one ligand and a pyrrole moiety of the opposite ligand.

acetophenone),[2] which are observed to be involved in π stacking in the solid state, undergo a significant upfield shift in the complexes. This upfield shift is consistent with the existence of the stacking interactions in solution.[18] While in the solid state some rings are more closely stacked than

(18) Martin, C. B.; Mulla, H. R.; Willis, P. G.; Cammers-Goodwin, A. *J. Org. Chem.* **1999**, *64*, 7802–7806.

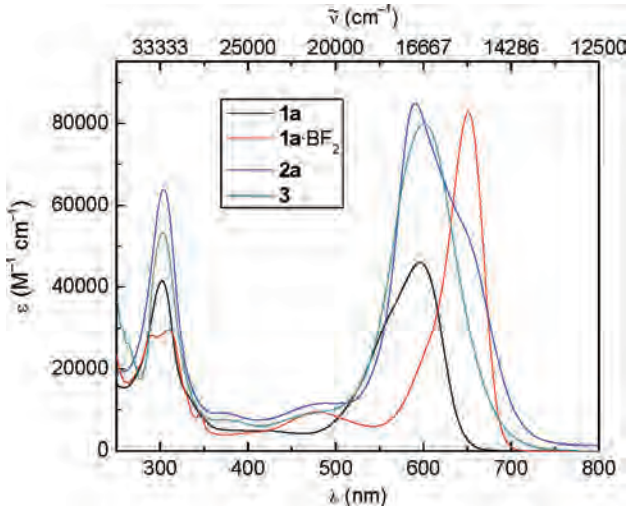

Figure 4. Absorption spectra of **1a**, **2a**, and **3**, recorded in THF at 298 ± 2 K. For comparison, the absorption spectrum of difluoroboron azadipyrromethane **1a**·BF_2 is illustrated.

others, the (room temperature) NMR spectrum is perfectly symmetric, indicating that the structure is fluxional on the NMR time scale, giving an "average" structure in which all rings undergo the same degree of π stacking.

Optical Absorption Spectra. One of the most attractive features of azadipyrromethenes is their intense absorption in the red region of the spectrum, making them ideally suited for in vivo applications.[1–6] Free azadipyrromethenes **1a**−**c** show two distinct absorption bands of nearly equal intensity, one at ca. 600 nm and the other at ca. 300 nm. UV/vis absorption spectra for the complexes were measured and compared to the free azadipyrromethene ligands. Figure 4 overlays UV/vis absorption spectra for **2a**, **3**, and their parent ligand, **1a**, measured in THF at micromolar concentrations. Also inlaid is the absorption spectrum of the boron adduct **1a**·BF_2. Spectra of difluoroboron azadipyrromethenes have been extensively discussed.[2] Upon binding of the Lewis acidic fragment BF_2^+, the absorption maximum of the lowest-energy transition red-shifts some 57 nm and its molar absorptivity increases by 31%.

Complexes **2a** and **3** show marked changes in their absorption spectra relative to the free ligand **1a**, notably in the red region. In **1a**, the absorption maximum occurs at 596 nm, with $\epsilon = 46\,000$ M^{-1} cm^{-1} (extinction coefficients are normalized to molar concentrations of compounds, not to the number of ligands). In **2a**, λ_{max} blue-shifts slightly to 591 nm, but the absorption intensity nearly doubles to 85 000 M^{-1} cm^{-1}. Also readily apparent in the spectrum of **2a** is the development of a second absorption transition, which appears as a shoulder at $\lambda = 640$ nm, $\epsilon = 58\,000$ M^{-1} cm^{-1}. Thus, even though λ_{max} is slightly blue-shifted in **2a**−**c** relative to **1a**−**c**, the zinc(II) complexes absorb a much wider range of red wavelengths because of this second absorption transition. Gaussian deconvolution of the 500–800 nm region of the spectra of **1a** and **2a** indicates maxima at 563.9 and 602.4 nm (**1a**) and 590.1 and 642.7 nm (**2a**) (Figures S3 and S4 in the Supporting Information). The spectrum of **3** likewise shows an intensified red-region absorption with $\lambda_{max} = 601$ nm and $\epsilon = 80\,000$ M^{-1} cm^{-1}. However, there is no second distinct transition resolved as is in **2a**. Careful examination of the low-energy band in **3** shows that it is unsymmetrical and tails out into the red region, possibly indicating a second, unresolved transition at redder wavelengths. The spectra of both **2a** and **3** show low-intensity bands near 374 and 475 nm. The wavelength of the other, near-UV absorption peak (ca. 300–320 nm) is largely unshifted, changing by only 1–2 nm in the complexes relative to free ligands, with the molar absorptivity also increasing. Table 3 summarizes optical absorption data for all compounds.

Table 3. Summary of UV/Vis Absorption Wavelengths (nm) and Molar Absorptivities (M^{-1} cm^{-1}) for Ligands and Complexes

	λ_{max}, ϵ = near-UV	λ_{max}, ϵ = red	λ, ϵ = shoulder peak
1a	302, 42 000	596, 46 000	
1b	318, 32 000	620, 43 000	
1c	301, 34 000	607, 42 000	
2a	304, 64 000	591, 85 000	640, 58 000
2b	321, 58 000	612, 86 000	670, 55 000
2c	301, 60 000	598, 85 000	645, 62 000
3	303, 53 000	601, 80 000	

The spectra of **2b** and **2c** are analogous to that of **2a**. Methoxy substitution on either the proximal or remote phenyl rings bathochromically shifts the low-energy absorptions relative to the parent tetraphenyl ligand and complex. When the methoxy substituent is distal to the chelating nitrogens, as in **1c** and **2c**, the corresponding absorptions shift by only 7–9 nm relative to **1a** and **2a**. However, in **1b** and **2b**, with the methoxy group proximal to the chelating nitrogens, the change is greater and the correlated absorption peaks red-shift by 20–30 nm relative to **1a** and **2a**.

The bis(azadipyrromethene)zinc(II) and -mercury(II) complexes are nonemissive. Free ligands **1a**−**c** are weak emitters, with quantum yields of emission of 0.014 (**1b**) and smaller. BF_2 chelates of **1a**−**c** are highly emissive, with $\Phi_f = 0.34$, 0.36, and 0.23, respectively. [2] Monoazadipyrromethene coinage metal complexes also emit, albeit weakly.[17] However, the zinc(II) and mercury(II) complexes show no emission when excited anywhere within the absorption profile. Rotation of the pendant phenyl groups may induce nonradiative decay, and luminescence from group 12 complexes of rigidified azadipyrromethenes may be realizable.[4]

Calculations. Semiempirical molecular orbital calculations have been undertaken to rationalize the canted structure of bis(azadipyrromethene) chelates, where the conjugated ligand backbones stray from perpendicularity. Geometries of **2a**−**c** were optimized within the AM1 Hamiltonian[19,20] beginning from crystal structures (**2a** and **2c**) or from an idealized D_{2d} geometry (**2b**). Symmetry was imposed during all geometry optimization. All canted, D_2-symmetric structures are potential energy minima by harmonic frequency calculations. The idealized D_{2d}-symmetric structures have 8 (**2a** and **2b**) or 12 (**2c**) imaginary frequencies and are nonstationary geometries. Two views of optimized **2a** appear in Figure 5a. Optimization of the zinc(II) complex of the unsubstituted azadipyrromethene produced an energy minimum having perfect D_{2d} symmetry (i.e., the planes of the ligand backbones

(19) Dewar, M. J. S.; Zoebisch, E. G.; Healy, E. F.; Steward, J. J. P. *J. Am. Chem. Soc.* **1985**, *107*, 3902–3909.
(20) Dewar, M. J. S.; Merz, K. M., Jr. *Organometallics* **1988**, *7*, 522–524.

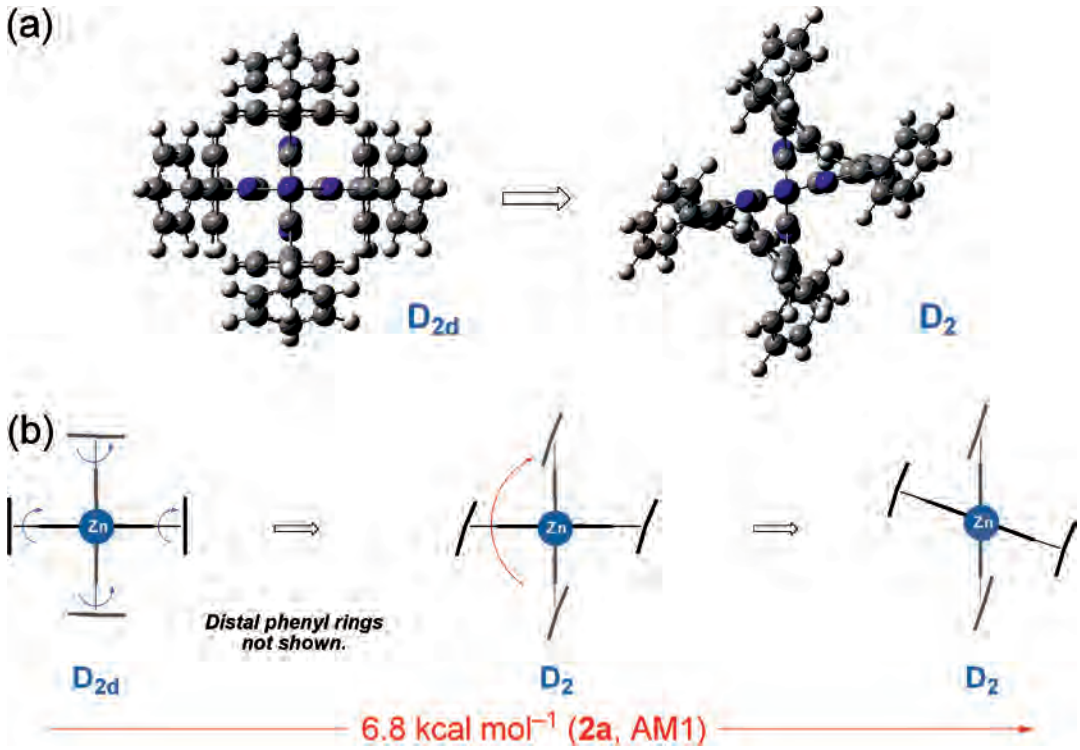

Figure 5. (a) Optimized (AM1) structures of D_{2d} and D_2 structures of **2a**. (b) Cartoon diagrams describing ligand canting in bis(azadipyrromethene)zinc(II) complexes. Canting in mercury complex **3** is similar.

are orthogonal). This result indicates that the observed ligand canting is not metal-imposed, as is expected for d^{10} metal centers.

The optimized geometry as depicted in Figure 5a is congested and difficult to apprehend. Figure 5b depicts the ligand canting in cartoon form. The proximal benzene rings (i.e., the phenyl substituents nearer to the metal center) rotate by the same angle and in the same direction. The opposing azadipyrromethene ligand also tilts in the same direction, as if in response to the initial leaning of the proximal phenyls. The depiction in Figure 5b is not intended as a mechanism for canting but as an aid in visualizing the geometries of the new complexes. Figure 5b indicates that the energy of the $D_{2d} \rightarrow D_2$ distortion, as calculated by AM1, is 6.8 kcal mol^{-1} for **2a**; corresponding figures are 14.9 kcal mol^{-1} (**2b**) and 15.2 kcal mol^{-1} (**2c**). A third process might be added to the schematic of Figure 5b: formation of a π-stacking interaction between the pyrrolyl ring of one ligand and a proximal phenyl of the opposite ligand. The semiempirical calculations herein fail to reproduce this interaction, presumably for lack of an adequate treatment of dispersion.[21] Present indications are that azadipyrromethene complexes are much given to π-stacking.[17] Such interactions are abundantly precedented outside of nucleic acid chemistry; they result primarily from favorable electrostatics.[22–26]

Recent investigations of azadipyrromethene complexes[1–6] have emphasized the ligands' optical absorption properties. The INDO/S configuration interaction singles protocol[27–34] was applied to bis(azadipyrromethene)zinc(II) complexes. Calculations on the experimental geometries[35] of **2a** and **2c**, as opposed to AM1-optimized structures, afforded better fidelity to the experimental absorption spectra. Implicit THF solvation was included using a self-consistent reaction field method.[36]

The calculations indicate that the intense absorption features between ca. 500 and 800 nm (Figure 4) represent several overlapping optically allowed transitions. A sizable energy gap, ca. 7800 cm^{-1}, separates these low-lying states from the next higher-energy singlets. Agreement with the observed absorption spectra is fair. The shoulder observed

(21) Cramer, C. J. *Essentials of Computational Chemistry: Theories and Models*, 2nd ed.; Wiley: New York, 2004; p 149.
(22) Williams, V. E.; Lemieux, R. P.; Thatcher, G. R. J. *J. Org. Chem.* **1996**, *61*, 1927–1933.
(23) Zhang, J.; Moore, J. S. *J. Am. Chem. Soc.* **1992**, *114*, 9701–9702.
(24) Cozzi, F.; Cinquini, M.; Annuziata, R.; Siegel, J. S. *J. Am. Chem. Soc.* **1993**, *115*, 5330–5331.
(25) Newcomb, L. F.; Gellman, S. H. *J. Am. Chem. Soc.* **1994**, *116*, 4993–1994.
(26) Phillip, D.; Gramlich, V.; Seiler, P.; Diederich, F. *J. Chem. Soc., Perkin Trans. 2* **1995**, 875–886.
(27) Ridley, J.; Zerner, M. C. *Theor. Chim. Acta* **1973**, *32*, 111–134.
(28) Zerner, M. C.; Loew, G. H.; Kirchner, R. F.; Mueller-Westerhoff, U. T. *J. Am. Chem. Soc.* **1980**, *102*, 589–599.
(29) Zerner, M. C. *Rev. Comput. Chem.* **1991**, *2*, 313–366.
(30) Martin, C. H.; Zerner, M. C. *Inorganic Electronic Structure and Spectroscopy*; Wiley-Interscience: New York, 1999; Vol. *1*, pp 555–660..
(31) Thompson, M. A.; Zerner, M. C. *J. Am. Chem. Soc.* **1991**, *113*, 8210–8215.
(32) Thompson, M. A.; Glendening, E. D.; Feller, D. *J. Phys. Chem.* **1994**, *98*, 10465–10476.
(33) Thompson, M. A.; Schenter, G. K. *J. Phys. Chem.* **1995**, *99*, 6374–6386.
(34) Thompson, M. A. *J. Phys. Chem.* **1996**, *100*, 14492–14507.
(35) Non-hydrogen atom positions are those determined crystallographically; bond lengths to hydrogen atoms were optimized with AM1, with all other atoms being frozen.
(36) Karelson, M. M.; Zerner, M. C. *J. Phys. Chem.* **1992**, *96*, 6949–6957.

Table 4. One-Electron Components of Low-Energy, Optically Allowed Transitions in Bis(azadipyrromethene)zinc Complexes As Calculated within the INDO/S CIS Approximation[a]

energy (nm)	oscillator strength[b]	principal orbital contributions	interconfigurational oscillator strength[b]
		Compound **2a**	
685.8	0.4094	LUMO+1 (b_3) ← HOMO−1 (a)	0.2686
		LUMO (b_2) ← HOMO (b_1)	0.2464
595.3	0.1043	LUMO (b_2) ← HOMO−1 (a)	1.2769
		LUMO+1 (b_3) ← HOMO (b_1)	1.1936
581.9	0.0727	LUMO+1 (b_3) ← HOMO−1 (a)	0.2686
		LUMO (b_2) ← HOMO (b_1)	0.2464
535.4	2.3447	LUMO (b_2) ← HOMO−1 (a)	1.2769
		LUMO + 1 (b_3) ← HOMO (b_1)	1.1936
		Compound **2c**	
681.8	0.4418	LUMO+1 (b_3) ← HOMO−1 (a)	0.3584
		LUMO (b_2) ← HOMO (b_1)	0.3036
585.9	0.0466	LUMO (b_2) ← HOMO−1 (a)	1.2322
		LUMO+1 (b_3) ← HOMO (b_1)	1.1481
564.8	0.1465	LUMO+1 (b_3) ← HOMO−1 (a)	0.3584
		LUMO (b_2) ← HOMO (b_1)	0.3036
545.3	2.3098	LUMO (b_2) ← HOMO−1 (a)	1.2322
		LUMO+1 (b_3) ← HOMO (b_1)	1.1481

[a] Calculations employed the crystallographic geometry with hydrogens in AM1-optimized positions. All transitions are to ^{1}B states. [b] Oscillator strengths were calculated with use of the dipole length operator.[31]

at 643 nm (from Gaussian deconvolution) in the spectrum of **2a** is 39 nm blue-shifted from the calculated transition at 682 nm, whereas the predominant transition at 590 nm is red-shifted by 45 nm from the calculated value. Some assignments can be ventured.

Table 4 summarizes principal components of calculated singlet–singlet excitations and the associated oscillator strengths. Figure 6 depicts optically allowed transitions among low-lying singlet states of **2a** alongside plots of several pertinent orbitals. The calculations find that those transitions with the greatest oscillator strengths have heavy contributions from the one-electron b_2 LUMO ← a HOMO−1 and b_3 LUMO+1 ← b_1 HOMO excitations (both to $^1B_2$ states in D_2 symmetry). The one-electron b_2 LUMO ← b_1 HOMO transition has roughly 20% of the oscillator strength of either of these other one-electron excitations. The ligand orbitals appearing in Figure 6 are recognizable descendents of the molecular orbitals of the C_{2v}-symmetric azadipyrromethene anion, as diagrammed in the Supporting Information. The b_1 HOMO and a HOMO−1 of **2a** are both related to the a_2 HOMO of the free ligand. The HOMO and HOMO−1 differ in that the orbital phase on the lower azadipyrromethene (as shown in Figure 6, left) reverses sign. The b_2 LUMO and b_3 LUMO+1 are composed of the individual LUMOs of the free ligand. In Figure 6, right, the phase of the upper ligand alternates sign between the LUMO and LUMO+1. The figure also indicates the relatively greater oscillator strength associated with the b_2 LUMO ← a HOMO−1 and b_3 LUMO+1 ← b_1 HOMO one-electron transitions, compared to other single transitions among the frontier orbitals. These promotions contribute significantly to the calculated transitions, which themselves are linear combinations of one-electron excitations. Whereas the low-energy transitions of monoazadipyrromethene complexes are predominated by two one-electron transitions,[17] those of zinc(II) bis(azadipyrromethenes) are composed of four.

At higher energies, between ca. 350 and 500 nm, numerous transition energies occur, all of comparatively slight oscillator strength. The INDO/S calculations find these to be ligand-centered, as expected for complexes of zinc(II) and, by extension, mercury(II). Configuration interaction in these higher-energy states is extensive, and the calculated excitations are combinations of one-electron promotions. An intense feature occurs near 300 nm in all complexes. A magnified view of this part of the spectrum appears in Figure 7. The absorption wavelengths of these features are insensitive to metal-ion complexation (or its lack); they do vary with ring substitution on the pendant phenyl groups. INDO/S CI computations on **2a** and **2c** reproduce these near-UV features and indicate them to be ligand-based. For **2a**, absorptions are calculated at 309.4 and 299.6 nm, respectively; both are excitations to B_1 states. In compound **2c**, where methoxy groups occupy the para positions of the remote phenyl rings, the corresponding $^1B_1$← ^1A transition is calculated at 300.0 nm. The dependence of the higher-energy (near 300 nm) features on ring substitution indicates phenyl group participation, and the INDO/S CI calculations indeed suggest a contribution from pπ orbitals on these substituents.

Conclusions

Syntheses and characterization of d^{10} zinc(II) and mercury(II) complexes of azadipyrromethene ligands are demonstrated. The transition-metal coordination chemistry of these interesting ligands, which are noted for their intense absorption in the red region of the spectrum, has remained under-explored. The complexes described herein adopt a pseudotetrahedral geometry in the solid state, with a significant distortion from D_{2d} symmetry. Semiempirical molecular orbital (AM1) calculations indicate that electronic relaxation partly drives these distortions. They fail to account for intramolecular ligand−ligand π-stacking, which reinforces ligand canting ($D_{2d} \rightarrow D_2$ symmetry). NMR spectra suggest that these π interactions are maintained in solution. The crystal structures also show that the meso nitrogen deviates from perfect sp^2 geometry upon metal binding. One of the more prominent features of these complexes is their optical absorption profiles. In the zinc(II) complexes, the molar absorptivity for the peak absorbance nearly doubles relative to the respective free ligand, and a second distinct absorption transition is evident at longer wavelengths. The mercury(II) complex also displays an intensified absorption in the red region, but only one such band is observed. Transition-metal chelation offers a novel means of tuning the absorption properties of azadipyrromethenes, an emerging class of organic fluorophores with several potential in vivo applications.

Experimental Section

General Procedures. $Zn(OAc)\cdot 2H_2O$ (OAc = acetate) and all solvents were obtained commercially and used without purification. Tetraarylazadipyrromethene ligands[2] **1a**−**c** were prepared as previously described. ^{1}H NMR spectra were recorded on a Varian AS-

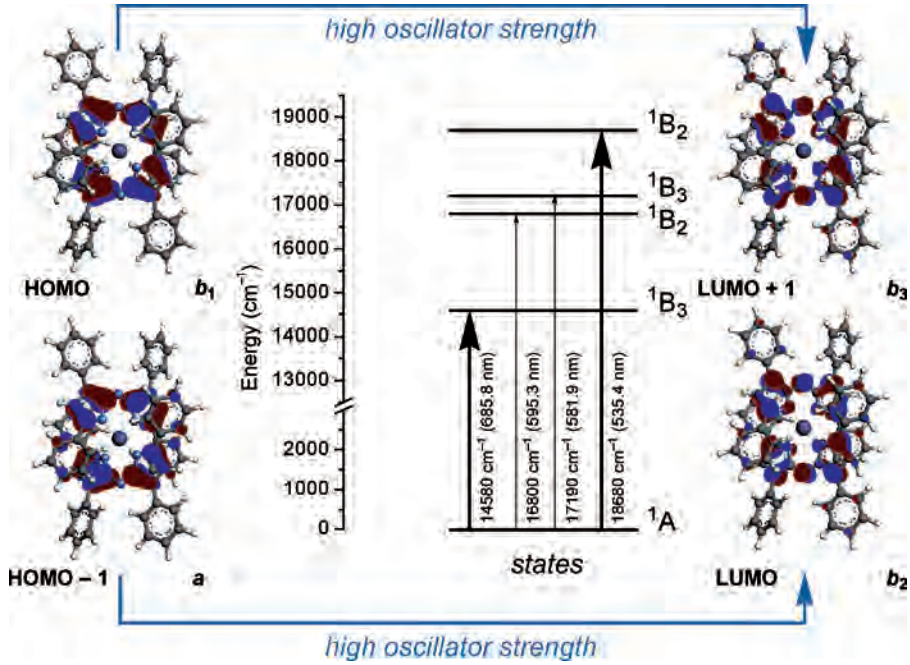

Figure 6. Calculated (INDO/S, CIS) singlet transitions of **2a** in the crystallographically determined geometry. Hydrogens are in AM1-optimized positions. Darker arrows indicate excitations of higher calculated oscillator strength. THF solvation is included implicitly in a self-consistent reaction field model. Left and right: frontier orbitals as indicated; 0.03 au contour level. Interconfigurational transitions having substantial one-electron oscillator strength (i.e., LUMO ← HOMO−1 and LUMO+1 ← HOMO) are indicated with blue arrows along the outside of the figure; calculated excitation transitions (black arrows, center) are linear combinations of these interconfigurational, one-electron promotions.

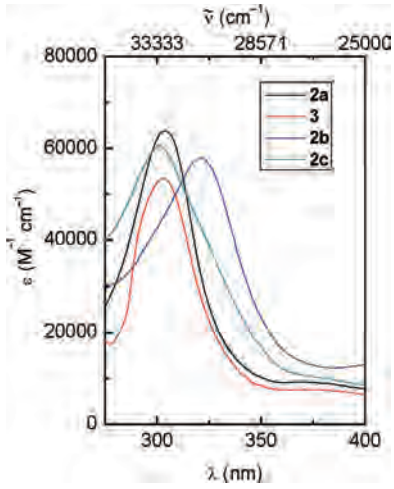

Figure 7. Absorption features near 300 nm of bis(azadipyrromethene) complexes, in THF.

400 spectrometer operating at 400 MHz. Chemical shifts are referenced to residual solvent resonances. UV/vis absorption spectra were recorded on a Cary 5G spectrophotometer in tetrahydrofuran (THF) solutions at micromolar concentrations at which all new compounds obeyed Beer's law.

[(3,5-Diphenyl-1*H*-pyrrol-2-yl)(3,5-diphenylpyrrol-2-ylidene)amine]zinc(II) (2a). To a solution of $Zn(OAc)_2 \cdot 2H_2O$ (12 mg, 0.055 mmol) in 10 mL of THF was added a solution of **1a** (50 mg, 0.11 mmol) in 10 mL of THF. The resulting solution was stirred at room temperature overnight. The solvent was removed by rotary evaporation, and the resulting residue was taken up in ca. 5 mL of CH_2Cl_2 and filtered through Celite. The solvent was removed by rotary evaporation to give the product as a metallic, dark-colored solid. The product was recrystallized from THF by vapor diffusion of pentane at room temperature. Yield: 45 mg (84%). ^{1}H NMR ($CDCl_3$): δ 7.86 (dd, 8H), 7.49 (dd, 8H), 7.36–7.42 (m, 12H), 7.06–7.13 (m, 12H), 6.71 (s, 4H) ppm. UV/vis (THF): λ (ϵ) 304 (64 000), 591 (85 000), 640(sh) (58 000) nm. Anal. Calcd for $C_{64}H_{44}N_6Zn$: C, 79.87; H, 4.61; N, 8.73. Found: C, 79.74; H, 4.38, N, 8.54.

{[5-(4-Methoxyphenyl)-3-phenyl-1*H*-pyrrol-2-yl][5-(4-methoxyphenyl)-3-phenylpyrrol-2-ylidene]amine}zinc(II) (2b). To a solution of $Zn(OAc)_2 \cdot 2H_2O$ (12 mg, 0.055 mmol) in 10 mL of THF was added a solution of **1b** (54 mg, 0.11 mmol) in 10 mL of THF. The resulting solution was stirred at room temperature for 12 h. All volatiles were removed by rotary evaporation; the resulting residue was dried in vacuo, then taken up in ca. 5 mL of CH_2Cl_2, and filtered through Celite. The solvent was evaporated by rotary evaporation to give a dark-colored solid, which was recrystallized from THF by vapor diffusion of pentane at room temperature to give the product as a fibrous, purple solid. Yield: 52 mg (90%). ^{1}H NMR ($CDCl_3$): δ 7.90 (dd, 8H), 7.44 (dd, 8H), 7.35–7.44 (m, 12H), 6.71 (s, 4H), 6.61 (d, J = 8.8 Hz, 8H), 3.37 (s, 12H) ppm. UV/vis (THF): λ (ϵ) 321 (58 000), 612 (86 000), 673(sh) (55 000) nm. Anal. Calcd for $C_{68}H_{52}N_6O_4Zn$: C, 75.44; H, 4.84; N, 7.76. Found: C, 74.85; H, 4.28, N, 7.67.

{[3-(4-Methoxyphenyl)-5-phenyl-1*H*-pyrrol-2-yl][3-(4-methoxyphenyl)-5-phenylpyrrol-2-ylidene]amine}zinc(II) (2c). To a solution of $Zn(OAc)_2 \cdot 2H_2O$ (11 mg, 0.050 mmol) in 10 mL of THF was added a solution of **1c** (51 mg, 0.10 mmol) in 10 mL of THF. The resulting solution was stirred at 40 °C for 12 h. The reaction mixture was allowed to cool to room temperature, and all volatiles were removed by rotary evaporation. The resulting solid was taken up in ca. 10 mL of CH_2Cl_2 and filtered through Celite. The solvent was removed by rotary evaporation to give a black solid, which was recrystallized from THF by vapor diffusion of pentane at room temperature to give the product as a crystalline, gold-colored solid. Yield: 29 mg (54%). ^{1}H NMR ($CDCl_3$): δ 7.83 (d, J = 9.2 Hz, 8H), 7.47 (dd, 8H), 7.02–7.10 (m, 12H), 6.97 (d, J = 8.8 Hz, 8H), 6.62 (s, 4H), 3.92 (s, 12H) ppm. UV/vis (THF):

λ (ϵ) 301 (60 000), 598 (85 000), 645(sh) (62 000) nm. Anal. Calcd for $C_{68}H_{52}N_6O_4Zn$: C, 75.44; H, 4.84; N, 7.76. Found: C, 74.55; H, 4.29; N, 7.72.

[(3,5-Diphenyl-1*H*-pyrrol-2-yl)(3,5-diphenylpyrrol-2-ylidene) amine]mercury(II) (3). To a suspension of $Hg(OAc)_2$ (47 mg, 0.15 mmol) in ~6 mL of THF was added solid **1a** (88 mg, 0.20 mmol) followed by an additional 2 mL of THF. The reaction was stirred at room temperature for 24 h, yielding a bright-blue solution. The solvent was removed via rotary evaporation, and the resulting residue was extracted into toluene (~40 mL) and filtered through Celite. Removal of the solvent via rotary evaporation gave a shiny red residue, which was triturated with pentane to afford a dark-red solid. The solid was collected, washed with 2 × 10 mL of pentane, and dried in vacuo to give the product in pure form as judged by NMR. Yield: 66 mg (61%). Analytically pure product was obtained by recrystallization of the product from a concentrated THF solution via vapor diffusion of pentane. ^{1}H NMR ($CDCl_3$): δ 7.79 (dd, 8H), 7.52 (dd, 8H), 7.36–7.38 (m, 12H), 7.10–7.13 (m, 12H), 6.93 (s, 4H) ppm. UV/vis (THF): λ (ϵ) 303 (53 000), 601 (80 000) nm. Anal. Calcd for $C_{64}H_{44}N_6Hg$: C, 70.03; H, 4.04; N, 7.66. Found: C, 68.76; H, 4.22; N, 6.98.

Calculations. Semiempirical molecular orbital calculations used the AM1 Hamiltonian[19,20] and parameters as codified within the program *Gaussian03*.[37] All calculations were spin-restricted with singlet spin multiplicity. Geometries were optimized using the Berny algorithm within redundant internal coordinates. Symmetry (D_{2d} or D_2) was imposed on all optimizations. Harmonic frequency calculations verified converged structures of D_2 symmetry to be energy minima.

Configuration-interaction singles (CIS) calculations were performed on the crystallographically determined geometries of **2a** and **2c** (except that C−H bond lengths are AM1-optimized values) using the intermediate neglect of the differential overlap (INDO/S) model of Zerner and co-workers,[27–34] as implemented in the program *ArgusLab 4.0.1*.[38] The active space consisted of the 10 highest-occupied and 10 lowest-unoccupied spin-restricted orbitals using a minimal-valence STO-6G basis set. Two-electron Coulomb integrals were calculated with the Weiss parameter set to 1.2. Implicit THF solvation (ϵ = 7.565; n_D = 1.408, 20 °C) was incorporated through a self-consistent reaction field model where excitation is instantaneous and only the electronic polarization of the solvent responds to the excited-state charge distribution.

Acknowledgment. The authors thank Case Western Reserve University and the donors of the Petroleum Research Fund, administered by the American Chemical Society (42312-G3 to T.G.G.) for support. T.S.T. thanks the Case Western Reserve University SOURCE program for funding. The diffractometer was funded by NSF Grant CHE0541766. We thank L. Gao and M. A. Peay for experimental assistance.

Supporting Information Available: X-ray crystallographic data in CIF format, optical absorption spectra for **1b**, **2b**, **1c**, and **2c**, calculated transition energies, HOMO and LUMO, and AM1-optimized geometries. This material is available free of charge via the Internet at http://pubs.acs.org.

IC701190G

(37) Frisch, M. J.; Trucks, G. W.; Schlegel, H. B.; Scuseria, G. E.; Robb, M. A.; Cheeseman, J. R.; Montgomery, Jr. J. A.; Vreven, T.; Kudin, K. N.; Burant J. C.; Millam, J. M.; Iyengar, S. S.; Tomasi, J.; Barone, V.; Mennucci, B.; Cossi, M.; Scalmani, G.; Rega, N.; Petersson, G. A.; Nakatsuji, H.; Hada, M.; Ehara, M.; Toyota, K.; Fukuda, R.; Hasegawa, J.; Ishida, M.; Nakajima, T.; Honda, Y.; Kitao O.; Nakai, H.; Klene, M.; Li, X.; Knox, J. E.; Hratchian, H. P.; Cross, J. B.; Bakken, V.; Adamo, C.; Jaramillo, J.; Gomperts, R.; Stratmann R. E.; Yazyev O.; Austin A. J.; Cammi R.; Pomelli C.; Ochterski J. W.; Ayala P. Y.; Morokuma K.; Voth G. A.; Salvador P.; Dannenberg J. J.; Zakrzewski V. G.; Dapprich S.; Daniels A. D.; Strain M. C.; Farkas O.; Malick D. K.; Rabuck A. D.; Raghavachari K.; Foresman J. B.; Ortiz J. V.; Cui Q.; Baboul A. G.; Clifford S.; Cioslowski J.; Stefanov B. B.; Liu G.; Liashenko A.; Piskorz P.; Komaromi I.; Martin R. L.; Fox D. J.; Keith T.; Al-Laham M. A.; Peng C. Y.; Nanayakkara A.; Challacombe M.; Gill P. M. W.; Johnson B.; Chen W.; Wong M. W.; Gonzalez C.; and Pople J. A. *Gaussian 03*, revision D.01; Gaussian, Inc.: Wallingford, CT, 2004.

(38) Thompson, M. A. *ArgusLab 4.0*; Planaria Software LLC: Seattle, WA, http://www.arguslab.com.